

CHAPTER II. RESISTANCE TO SIGNAL ACTIVATION GOVERNS DESIGN FEATURES OF THE MAP KINASE SIGNALING MODULE

1. Abstract

Given its broad influence over numerous cell functions, redesigning the mitogen-activated protein (MAP) kinase signaling module would offer powerful means to engineer cell behavior. Early challenges include identifying quantitative module features most relevant to biological function and developing simple design rules to predictably modify these features. This modeling study delineates how features such as signal amplification, input potency and dynamic range of output may be tuned by manipulating chief module components. Importantly, the model construction identifies a metric of resistance to signal activation that quantitatively predicts module features and design trade-offs for broad perturbations in kinase and phosphatase expression. Its predictive utility extends to dynamic properties such as signal lifetime, which often dictates MAP kinase effect on cell function. Taken together, we propose that predictably altering MAP kinase signaling by tuning resistance is not only a feasible engineering strategy, but also one exploited by natural systems to allow each MAP kinase to exert pleiotropic effects in a context-dependent manner. External stimuli not only activate kinases, but also alter phosphatase expression and activity, thereby reconfiguring a single module for quantitatively distinct modes of signaling such as transient versus sustained dynamics, each with unique effects on cell function.

Stephen Chapman and Anand R. Asthagiri, *Bioengineering and Biotechnology*, © John Wiley & Sons, Inc, 2004. Reprinted with permission from Wiley-Liss, Inc. a subsidiary of Wiley & Sons, Inc.

2. Introduction

The MAP kinase family of serine/threonine protein kinases are found among species ranging from *S. pombe* to *H. sapiens* (Lewis et al., 1998; Pearson et al., 2001). In mammals, MAP kinases have been implicated in regulating cell migration, apoptosis, proliferation and differentiation. Because of its broad influence, establishing strategies to redesign MAP kinase signaling would offer powerful means to engineer cell behavior. Recently, conceptual understanding of how MAP kinase pathways utilize scaffolds to maintain fidelity of stimulus-response relationships was elegantly exploited to engineer an artificial scaffold that converts yeast cell response to α -factor from the natural mating response to an osmolarity-stress response (Park et al., 2003). Notably, the growing emphasis to transform conceptual description of signaling mechanisms into quantitative, dynamical models (Endy and Brent, 2001) would further expand the design space to include the possibility of quantitatively tuning information flow through signaling networks. This work focuses on early challenges to such quantitative redesign of the ubiquitous MAP kinase signaling module.

Most MAP kinases signal through a well-preserved mechanism, involving serial activation of a cascade of enzymes (Figure II-1). The wide recurrence of this cascade structure has garnered its label as a ‘signaling module’ and has raised interest in the inherent utility of its design. Classically, these cascades have been viewed as signal amplifiers (Pearson et al., 2001). Each active enzyme at the top of the cascade (E_1^*) activates several targets (E_2); and each of those activated target enzymes (E_2^*) would, in

turn, activate its own group of targets (E_3). Hence, magnitude amplification has been conjectured as a canonical function for enzyme cascades.

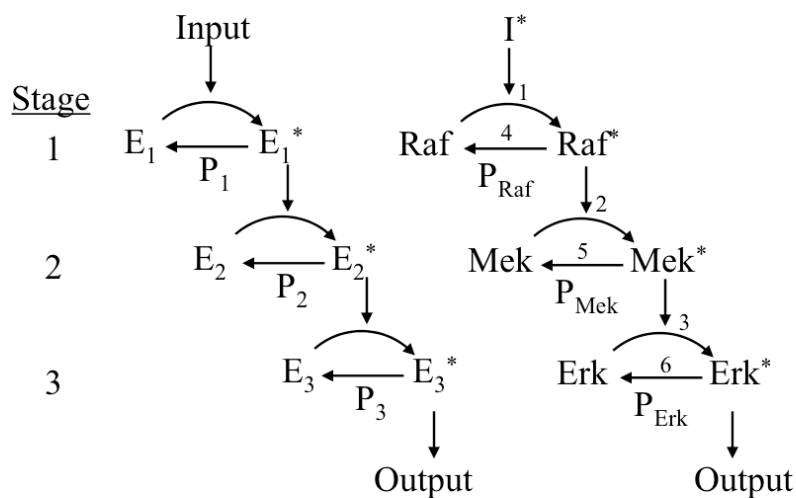


Figure II-1. Model schematic.

The MAP kinase module consists of a cascade of three kinases (E_i) and their counterpart phosphatases (P_i) as illustrated on the left. On the right, an example cascade is depicted: the Erk subfamily of MAP kinases is activated via the Raf-Mek-Erk cascade. An input initiates the cascade by activating the topmost kinase, while the module output is the number of active MAP kinase, in this case Erk. At each stage s , phosphatases catalyze the deactivation of kinases. More generally, at stage s an activated, upstream kinase (K_{s-1}) converts its substrate (K_s) from an inactive to active form. Meanwhile, phosphatases at each stage (P_s) deactivate the kinase. Although not depicted, each enzyme(E)-substrate(S) reaction involves the formation of an ES complex: $E + S \leftrightarrow ES \rightarrow E + P$.

Computational models offer a framework to examine such issues in a rigorous manner (Tyson et al., 2001). Inferring specific insight into the MAP kinase module from models of large-scale signaling networks is thwarted by the inclusion of numerous

mechanisms external to the cascade (Schoeberl et al., 2002). A complementary approach focuses on the module, typically represented by a cascade of three kinases counterbalanced by constitutive deactivation enzymes (phosphatases) at each level of the cascade (Ferrell, 1996). Such models and congruent experimental work in *Xenopus* oocyte extracts have demonstrated that mechanisms such as distributive, two-step kinase activation confers ultrasensitivity at each step of the cascade (Huang and Ferrell, 1996). Moreover, cascade structure helps to accumulate this ultrasensitivity from each stage, so that module output reveals switch-like, steady-state responses to changes in stimulus concentration (Brown et al., 1997; Ferrell, 1997). In addition, aforementioned scaffolding mechanisms have been analyzed using a similar modular approach, revealing that an optimal, intermediate scaffold concentration may be required for maximal signal (Levchenko et al., 2000).

In addition to delineating signaling properties conferred by cascade structure and its internal mechanisms, computational analysis is necessary to develop strategies to re-engineer this module toward novel performance objectives. In fact, the first challenge is to identify quantitatively the design objectives themselves, with focus on enhancing biological efficacy or altering the information content of this cascade. Here, we delineate how such design goals may be defined in terms of quantitative features of the module, including the threshold amount of input required to trigger the MAP kinase switch. Since signaling via the Erk subfamily of MAP kinases is required for proliferation (Pages et al., 1993), redesigning the Erk module to respond to lower input levels may improve cell sensitivity to a mitogenic factor. Such hyper-responsive, re-engineered cells may help to

reduce costs associated with growth factors necessary for *ex vivo* repopulation of tissue engineering scaffolds. Alternatively, in instances where the MAP kinase of interest, such as JNK, drives apoptosis or programmed cell death (Davis, 2000), it may be desirable to reduce its sensitivity to environmental stresses, with possible implications for cell culture maintenance in bioprocess applications.

Ultimately, even modules with altered sensitivity to stimulus must effectively communicate with downstream targets to elicit cellular response. In some instances, MAP kinase modules perform as a switch, shifting between on- and off-states (Huang and Ferrell, 1996). In order for this switch to impart disparate cellular responses, downstream effectors must clearly distinguish between on- and off-states. Thus, the module must communicate with output intensity of adequate dynamic range.

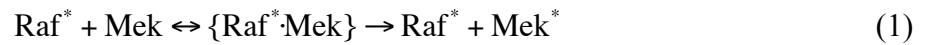
Finally, in addition to optimizing module communication with upstream input and downstream targets, it is desirable to tune the information content of the module itself. This information is often embedded in signal dynamics as in the case of Erk and JNK, whose transient activation has been linked to proliferation and survival, respectively, while sustained activation yields differentiation and apoptosis, respectively (Kao et al., 2001; Marshall, 1995; Roulston et al., 1998). Thus, tuning signal lifetime would offer control over cell fate, with direct implications for rationally designing therapeutic strategies that seek to revert pathological cell behavior. Of particular relevance are those disease states, such as cancer, in which aberrant MAP kinase signaling plays a significant, mechanistic role in leading to hyperproliferation and de-differentiation

(Lewis et al., 1998). This work delineates how these features—responsiveness to stimulus, range of output, and signal lifetime—and other quantitative attributes of the MAP kinase module may be re-engineered by manipulating experimentally-accessible system variables.

Importantly, a second challenge is to guide redesign of these quantitative features of information flow with *a priori* knowledge of potential consequences caused by specific manipulations. Our model construction identifies a metric of resistance to signal activation, which serves as such a predictive tool. Thus, the resistance effectively predicts both steady-state and dynamic features of the module for broad perturbations in kinase and phosphatase expression levels. Notably, these system variables are manipulable using established techniques, such as RNA interference, antisense RNA or exogenous overexpression from mammalian expression vectors, making the proposed redesign strategies practically feasible. Taken together, we propose that predictably altering MAP kinase signaling by tuning resistance is not only a practical engineering strategy, but also one exploited by natural systems to allow each MAP kinase to exert pleiotropic effects on cell behavior.

3. Model Development - Schematic and Equations

A first-level representation of the MAP kinase module involves three kinases in series, each activated by its predecessor. A schematic of such a cascade is shown in Figure II-1 for the Erk subfamily of MAP kinases. At each stage (s), there are two reactions ($i = s, s + 3$), one catalyzed by the upstream activator, and the other by the counteracting phosphatase. A representative pair ($i = 2, 5$) of reaction mechanisms for the second stage is given below:



where enzyme-substrate complexes are denoted by $\{\text{ES}\}$. For Reaction 1, the association of Raf^* and Mek is governed by the second-order rate constant $k_{+,2}$, while the first-order rate constant for dissociation of the complex is given by $k_{-,2}$. Finally, the rate of product formation from this enzyme-substrate complex is dictated by the constant $k_{\text{cat},2}$. In general, the rate constants of each enzyme-substrate reaction i is given by $k_{+,i}$, $k_{-,i}$, and $k_{\text{cat},i}$ where $i = 1 - 6$.

Taking into account the free (I), active (I^*) and Raf-associated ($I^* \cdot \text{Raf}$) forms of the input species, there are 17 components of the module. The amount of each of these components per cell were normalized by the total amount of each kinase and each phosphatase present in the system. Normalized, non-dimensional quantities are shown in italics to distinguish them from their dimensional counterparts:

$$\begin{aligned}
I &= \frac{I}{I_T} & I^* &= \frac{I^*}{I_T} \\
\{I^* \cdot Raf\} &= \frac{\{I^* \cdot Raf\}}{I_T} & Raf &= \frac{Raf}{Raf_T} \\
Raf^* &= \frac{Raf^*}{Raf_T} & \{Raf^* \cdot Mek\} &= \frac{\{Raf^* \cdot Mek\}}{Raf_T} \\
Mek &= \frac{Mek}{Mek_T} & Mek^* &= \frac{Mek^*}{Mek_T} \\
\{Mek^* \cdot Erk\} &= \frac{\{Mek^* \cdot Erk\}}{Mek_T} & Erk &= \frac{Erk}{Erk_T} \\
Erk^* &= \frac{Erk^*}{Erk_T} & P_{Rf} &= \frac{P_{Rf}}{P_{Rf,T}} \\
P_{Mk} &= \frac{P_{Mk}}{P_{Mk,T}} & P_{Ek} &= \frac{P_{Ek}}{P_{Ek,T}} \\
\{P_{Rf} \cdot Raf^*\} &= \frac{\{P_{Rf} \cdot Raf^*\}}{P_{Rf,T}} & \{P_{Mk} \cdot Mek^*\} &= \frac{\{P_{Mk} \cdot Mek^*\}}{P_{Mk,T}} \\
\{P_{Ek} \cdot Erk^*\} &= \frac{\{P_{Ek} \cdot Erk^*\}}{P_{Ek,T}} & &
\end{aligned} \tag{3}$$

Among the 17 non-dimensional variables, the fraction of input species in the active state (I^*) is provided as the driving function for the module. The values of the remaining 16 unknown dimensionless variables are determined partly by the following seven mass balances:

$$1 = I + I^* + \{I^* \cdot Raf\} \tag{4}$$

$$1 = Raf + Raf^* + \kappa_1 \{I^* \cdot Raf\} + \{Raf^* \cdot Mek\} + \pi_1 \{P_{Rf} \cdot Raf^*\} \tag{5}$$

$$1 = Mek + Mek^* + \kappa_2 \{Raf^* \cdot Mek\} + \{Mek^* \cdot Erk\} + \pi_2 \{P_{Mk} \cdot Mek^*\} \tag{6}$$

$$1 = Erk + Erk^* + \kappa_3 \{Mek^* \cdot Erk\} + \pi_3 \{P_{Ek} \cdot Erk^*\} \tag{7}$$

$$1 = P_{Rf} + \{P_{Rf} \cdot Raf^*\} \tag{8}$$

$$1 = P_{Mk} + \{P_{Mk} \cdot Mek^*\} \tag{9}$$

$$1 = P_{Ek} + \{P_{Ek} \cdot Erk^*\} \quad (10)$$

In conjunction with above, the following nine differential equations fully specify the behavior of the module:

$$\begin{aligned} \frac{dRaf^*}{d\tau} = & \frac{\kappa_1}{\tau_1} \{I^* \cdot Raf\} - \frac{\alpha_2}{\kappa_1 \kappa_2 \tau_2 \varepsilon_2} Raf^* Mek + \left(\frac{1}{\tau_2 \varepsilon_2} + \frac{1}{\tau_2} \right) \{Raf^* \cdot Mek\} - \dots \\ & \dots - \frac{\alpha_4 \pi_1}{\kappa_1 \tau_4 \varepsilon_4} Raf^* P_{Rf} + \frac{\pi_1}{\tau_4 \varepsilon_4} \{P_{Rf} \cdot Raf^*\} \end{aligned} \quad (11)$$

$$\begin{aligned} \frac{dMek^*}{d\tau} = & \frac{\kappa_2}{\tau_2} \{Raf^* \cdot Mek\} - \frac{\alpha_3}{\kappa_1 \kappa_2 \kappa_3 \tau_3 \varepsilon_3} Mek^* Erk + \left(\frac{1}{\tau_3 \varepsilon_3} + \frac{1}{\tau_3} \right) \{Mek^* \cdot Erk\} - \dots \\ & \dots - \frac{\alpha_5 \pi_2}{\kappa_1 \kappa_2 \tau_5 \varepsilon_5} Mek^* P_{Mk} + \frac{\pi_2}{\tau_5 \varepsilon_5} \{P_{Mk} \cdot Mek^*\} \end{aligned} \quad (12)$$

$$\frac{dErk^*}{d\tau} = \frac{\kappa_3}{\tau_3} \{Mek^* \cdot Erk\} - \frac{\alpha_6 \pi_3}{\kappa_1 \kappa_2 \kappa_3 \tau_6 \varepsilon_6} Mek^* P_{Mk} + \frac{\pi_3}{\tau_3 \varepsilon_3} \{P_{Mk} \cdot Mek^*\} \quad (13)$$

$$\frac{dRaf}{d\tau} = -\frac{\alpha_1}{\tau_1 \varepsilon_1} Raf I^* + \frac{\kappa_1}{\tau_1 \varepsilon_1} \{I^* \cdot Raf\} + \frac{\pi_1}{\tau_4} \{P_{Rf} \cdot Raf^*\} \quad (14)$$

$$\frac{dMek}{d\tau} = -\frac{\alpha_2}{\kappa_1 \tau_2 \varepsilon_2} Mek Raf^* + \frac{\kappa_2}{\tau_2 \varepsilon_2} \{Raf^* \cdot Mek\} + \frac{\pi_2}{\tau_5} \{P_{Mk} \cdot Mek^*\} \quad (15)$$

$$\frac{dErk}{d\tau} = -\frac{\alpha_3}{\kappa_1 \kappa_2 \tau_3 \varepsilon_3} Erk Mek^* + \frac{\kappa_3}{\tau_3 \varepsilon_3} \{Mek^* \cdot Erk\} + \frac{\pi_3}{\tau_6} \{P_{Mk} \cdot Mek^*\} \quad (16)$$

$$\frac{dP_{Rf}}{d\tau} = -\frac{\alpha_4}{\kappa_1 \tau_4 \varepsilon_4} P_{Rf} Raf^* + \left(\frac{1}{\tau_4 \varepsilon_4} + \frac{1}{\tau_4} \right) \{P_{Rf} \cdot Raf^*\} \quad (17)$$

$$\frac{dP_{Mk}}{d\tau} = -\frac{\alpha_5}{\kappa_1 \kappa_2 \tau_5 \varepsilon_5} P_{Mk} Mek^* + \left(\frac{1}{\tau_5 \varepsilon_5} + \frac{1}{\tau_5} \right) \{P_{Mk} \cdot Mek^*\} \quad (18)$$

$$\frac{dP_{Ek}}{d\tau} = -\frac{\alpha_6}{\kappa_1 \kappa_2 \kappa_3 \tau_6 \varepsilon_6} P_{Ek} Erk^* + \left(\frac{1}{\tau_6 \varepsilon_6} + \frac{1}{\tau_6} \right) \{P_{Ek} \cdot Erk^*\} \quad (19)$$

Appearing in Equations 4-19 are five classes of dimensionless parameters: π_s , κ_s , α_i , ε_i and τ_i . Their form, significance and range of values are summarized in Table II-1.

Simulations were performed using Matlab v. 6.1 and the *ode23s* and *fsolve* subroutines.

Table II-1. Five classes of dimensionless parameters specify module attributes.

Dimensionless Group	Significance	Symbol	Range of Values
P_s/K_s	amount of phosphatase relative to kinase at stage s	π_s	0.01-100
K_{s-1}/K_s	amount of upstream kinase relative to kinase at stage s	κ_s	0.3-3
$k_{+,i}I_T/k_{-,i}$	proportional to affinity for each enzyme-substrate pair i	α_i	0.1-10*
$k_{cat,i}/k_{-,i}$	efficiency with which each E'S complex i will form product versus dissociate in a non-productive fashion	ε_i	0.01-1*
$k_{cat,1}/k_{cat,i}$	characteristic time for product formation from each E'S complex i relative to characteristic time for product formation from $\{I^* \cdot Raf\}$	τ_i	0.1-10*

* Typical values for α_i , ε_i , τ_i were 0.6, 0.2 and 1, respectively (Asthagiri and Lauffenburger, 2001; Ferrell, 1996; Levchenko et al., 2000). For sensitivity analysis (see Appendix), these values were varied over two orders-of-magnitude near their typical value as indicated.

4. Results

4.1 Model construction identifies most tangible design opportunities

Our model construction by dimensional analysis and further parameter grouping reveals five classes of dimensionless parameters, which govern module behavior (Table II-1). Three of these parameter classes (α_i , ε_i , τ_i) involve rate constants, whose values are intrinsic properties of the reacting species. While these parameters clearly contribute to the quantitative properties of the module, more tangible design opportunities are offered by two other dimensionless groups. The first (π_s) represents the amount of phosphatase relative to kinase at each stage of the cascade. The second dimensionless group (κ_s) compares the expression level of an upstream kinase to the amount of its target at each stage. Thus, the values of these parameters are dictated by the expression levels of kinases and phosphatases, which are particularly attractive from a design perspective, since protein expression levels are readily adjustable in experimental systems using established techniques involving RNA interference, antisense RNA or mammalian expression vectors. Therefore, these two dimensionless groups are the focus of developing a redesign strategy.

4.2 Sustained input and steady-state features

Most mathematical treatments of the MAP kinase cascade utilize a step function for module input, which was initially employed here as well. Upstream components such as Ras, whose active form serves as input, may be expressed at levels as high as 10^5

copies per cell (Scheele et al., 1995). Therefore, non-zero values for the fraction of input species in its active state (I^*) may range between $10^{-5} - 10^0$. The module output is given by the fraction of Erk in its active state (Erk^*).

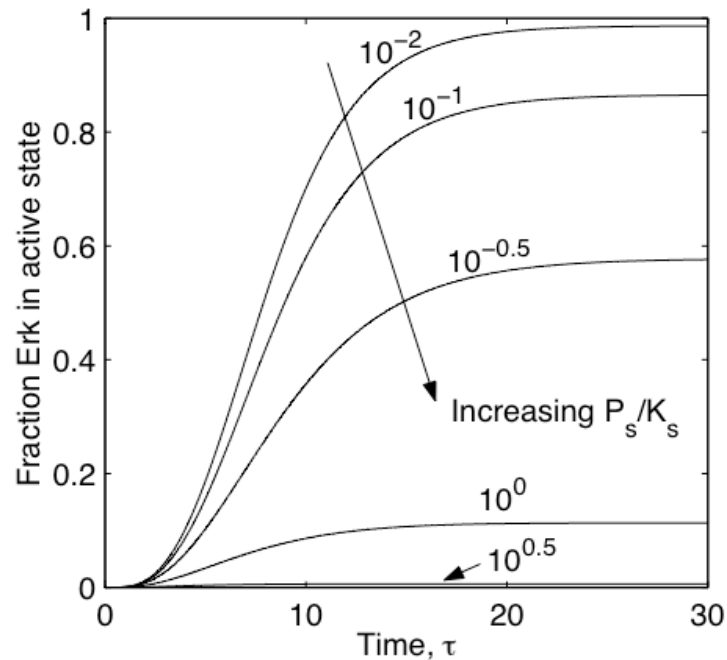


Figure II-2. Temporal profile of module output in response to a step input: the effect of varying the relative amount of phosphatase versus kinase.

Module was stimulated with a step input ($I^* = 10^{-0.5}$), and the fraction of Erk in its active state was tracked over time. Simulation was performed for different relative amounts of phosphatases compared to kinases ($\pi_s = 10^{-2} - 10^{0.5}$), while holding the ratio of upstream to downstream components fixed ($\kappa_s = 1$). Constitutive presence of phosphatases does not confer adaptation to a sustained input but affects level of steady-state output.

In the absence of negative feedback, no adaptation is observed in module output (Figure II-2), or among any of the upstream kinases (data not shown). Because signal adaptation does not occur, the steady-state behavior of this module was examined. For

this cascade, the steady-state fraction of Erk in its active state (module output) displays sigmoidal dependence on non-zero input amplitude (I^*) as shown in Figure II-3. This sigmoidal dependence has been shown to acquire steeper transition from minimal to maximal output, yielding switch-like behavior when kinase activation involves a two-step, distributive mechanism (Huang and Ferrell, 1996). Here, we consider three other properties—potency, range, and gain—which are crucial measures of this module's ability to propagate signal.

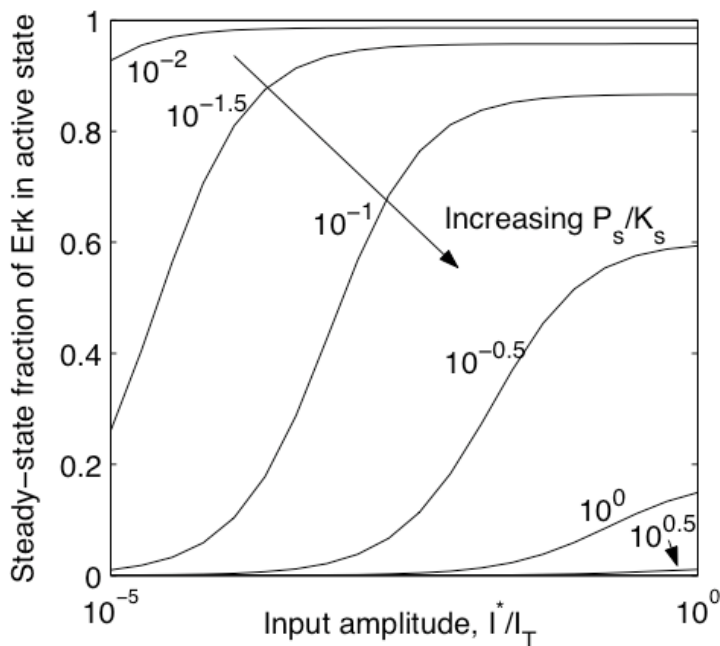


Figure II-3. Module dose-response to changes in the relative amount of phosphatase versus kinase.

The steady-state level of output was computed for different, non-zero input amplitudes for $\kappa_s = 1$. For intermediate ratios of phosphatase to kinase expression level ($\pi_s = 10^{-1}$), module output is a sigmoidal function of input amplitude. However, if kinases dramatically outnumber phosphatases or vice versa, module becomes insensitive to changes in input. In one extreme ($\pi_s \rightarrow 0$), module output is always maximal, even for minimal input; and, in the other extreme, module output is severely attenuated and unable to respond to even complete activation of input species.

4.2-1 Potency

Potency is a measure of how much input is required to elicit efficient module response. In experimental terms, stimulus potency is inversely related to the EC_{50} , which is the effective concentration of stimulus (typically, a ligand) required to attain half-maximal response (e.g., cell proliferation). By direct analogy, the potency of input to the MAPK module is $1/I_{50}^*$, where I_{50}^* is the input amplitude which promotes medium level of output. Module configurations that yield low values for I_{50}^* confer high potency to input as they enable low levels of input to efficiently propagate signal. We analyzed the dependence of input potency on module design, particularly focusing on components of the cascade which are most readily tunable experimentally.

The relative expression level of phosphatases to that of kinases ($P_s/K_s = \pi_s$) at each stage s dramatically affects input potency. This is most clearly revealed in Figure II-3 by the rightward shift in the “dose-response” curves as π_s is increased. In performing these simulations, the value of π_s was assumed to be equal for each stage s , largely due to the lack of experimental data that would suggest otherwise and in part to remain consistent with previous treatments of the MAP kinase module (Huang and Ferrell, 1996). For high π_s values, more phosphatases are present to deactivate kinases, thereby increasing the threshold amount of input required to elicit module response. Values for potency were calculated from dose-response curves, and its dependence on π_s is portrayed in Figure II-4. Consistent with the dose-response curves, input potency is a

monotonically decreasing function of π_s , with asymptotic upper and lower limits for low and high π_s values, respectively.

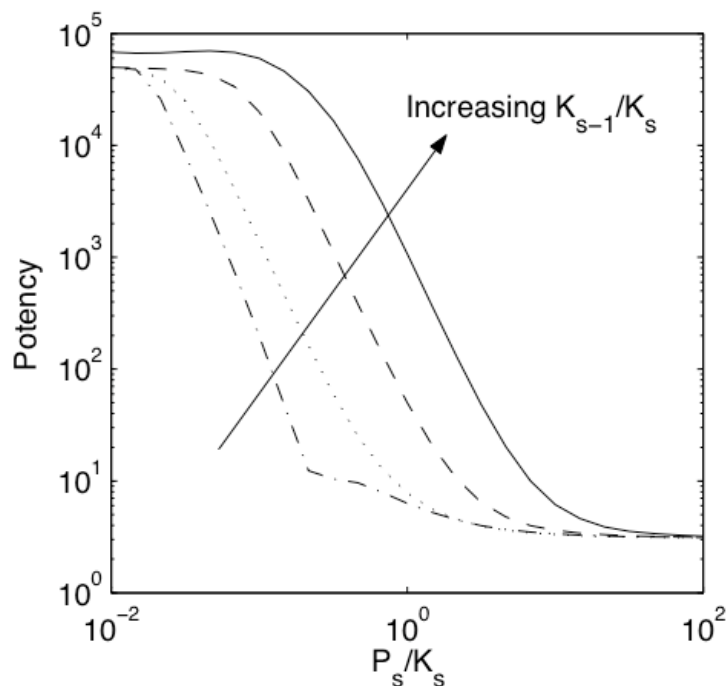


Figure II-4. Input potency.

Aspects of the module dose-response (Figure II-3) may be tuned by altering module configuration. The potency of the input is inversely related to the amount of input (I_{50}^*) required to attain average module output. For fixed (κ_s), an increase in the relative amount of phosphatases (π_s) reduces input potency, since more input is required to elicit half-maximal response. This trend is preserved for all $\kappa_s = 10^{-0.5}$ ($-\cdot-$), 10^0 (\cdots), $10^{0.5}$ ($--$), 10^1 ($-$). For fixed π_s , increasing the amount of upstream kinase relative to downstream target increases input potency.

In addition to phosphatase activity, signal generation at each stage of the cascade is determined by competing upstream activators. The net effect on module behavior may be evaluated by considering the π_s value in balance with the expression level of

upstream activators relative to its downstream target ($K_{s-1}/K_s = \kappa_s$). For fixed π_s , input potency is enhanced for higher relative expression levels of upstream activator (Figure II-4). For $\kappa_s > \pi_s$, upstream activation outweighs deactivation at each stage, enabling high module output even for low input.

4.2-2 Range of output

A second important attribute of the MAPK module is the range of output produced in response to a spectrum of non-zero input. This range is defined as the difference in output caused by full stimulation (i.e., all input species are active) versus minimal, non-zero input:

$$\text{range} = [Erk_{ss}^*]_{\text{max input}} - [Erk_{ss}^*]_{\text{min input}} \quad (20)$$

While model results depict output as a continuous function of input, discrete numbers of active Erk molecules serve as physiological module output. Thus, a module whose range of output is large would possess more intermediate values of output with which to convey “higher-grain” information to the next module.

Module range demonstrates biphasic dependence on π_s as shown in Figure II-5. For low π_s values, relatively few phosphatases are present to impede kinase activation. In this case, even minimal non-zero input activates all available kinases, precluding higher output in response to further increments in input. Meanwhile, at high π_s , intense phosphatase activity does not permit signal generation even at maximal stimulation, yielding no difference in output magnitude for low versus high input. Only at an optimal

intermediate π_s value, balanced phosphatase and upstream kinase activity enable a large range of output to changes in input stimulation. This balance is affected not only by the dimensionless parameter π_s , but also by the expression level of upstream activators relative to their downstream targets. Since upstream activation is enhanced for higher κ_s values, greater amount of phosphatases relative to kinases is required to balance activation. Thus, the π_s value needed to optimize module range increases for higher κ_s (Figure II-5).

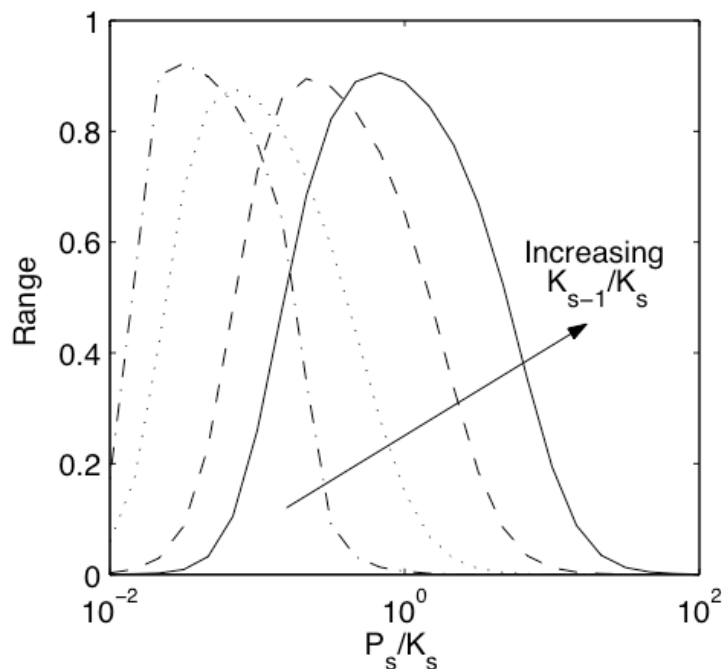


Figure II-5. Dynamic range of module output.

The dynamic range of output is the difference in module output in response to maximum input versus minimum, non-zero input. This range is a biphasic function of the ratio of phosphatase to kinase expression level (π_s) for $\kappa_s = 10^{-0.5}$ (---), 10^0 (···), $10^{0.5}$ (-·-), 10^1 (-). Thus, maximum range of output is achieved at an optimum π_s . An increase in the relative amount of upstream to downstream kinases shifts this optimum π_s value.

4.2-3 Signal amplification

While high-range modules “sense” low versus high input by producing maximally disparate output for these two extremes of stimulation, signal amplification quantifies the ability of the module to receive a certain amount of input and respond by generating even greater amount of output. Kinase cascades have been implicated as an optimal configuration to achieve such amplification (Pearson et al., 2001). In fact, amplification has been suggested to require greater amount of downstream kinase than upstream activator (i.e., $\kappa_s < 1$). Thus, signal transfer from Raf to Mek has been identified as an ideal point for amplification (Pearson et al., 2001) because Mek levels typically far exceed those of Raf (Ferrell, 1996). However, Mek and Erk are expressed typically at equimolar levels (Ferrell, 1996), suggesting that amplification may not be the chief purpose of this part of the cascade (Pearson et al., 2001).

We examined rigorously the dependence of signal amplification on relative expression level of upstream and downstream kinases (κ_s) and on the relative amount of phosphatases (π_s). The gain (Γ) in signal strength from input to output was quantified by the ratio of number of active Erk at steady-state to the level of input:

$$\Gamma = \left(\frac{Erk_{ss}^*}{I^*} \right) \left(\frac{Erk_T}{I_T} \right) \quad (21)$$

where Erk_{ss}^* and I^* are the fraction of each enzyme in their active state at steady-state and Erk_T and I_T are the total amount of each protein per cell. Thus, the module performs as an amplifier if $\Gamma > 1$ and as an attenuator if $\Gamma < 1$.

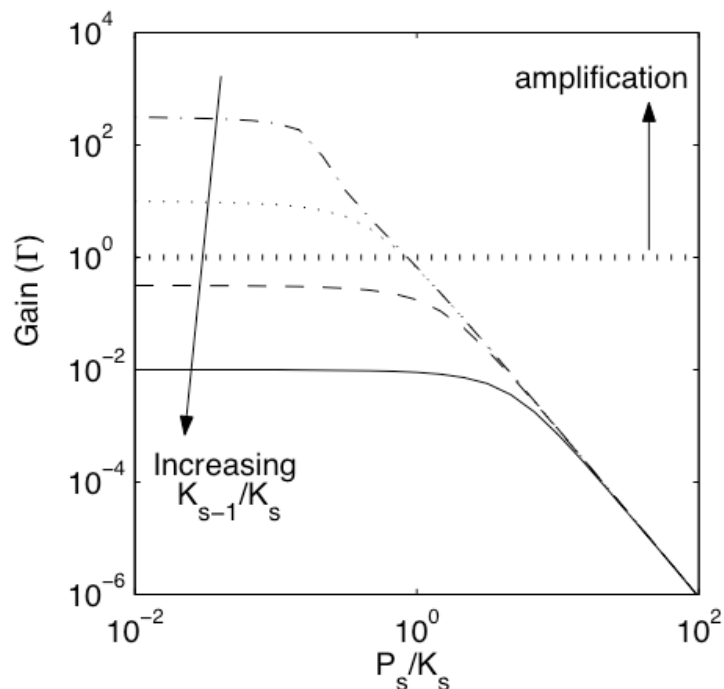


Figure II-6. Signal amplification versus attenuation.

For a given amount of input ($I^* = 10^{-0.5}$), the signal gain (Γ) is quantified as the ratio of number of active Erk species at steady-state to the number of active input species. The horizontal line ($\Gamma = 1$) demarcates regimes yielding signal amplification ($\Gamma > 1$) versus attenuation ($\Gamma < 1$). Even if downstream kinases outnumber upstream activators ($\kappa_s = 10^{-0.5}$ (---)), signal attenuation occurs for high relative expression of phosphatases. Conversely, at low π_s , amplification may occur even for equimolar expression of upstream and downstream kinases ($\kappa_s = 10^0$ (...)). If downstream kinases are outnumbered by upstream activators ($\kappa_s = 10^{0.5}$ (- -), 10^1 (-)), the MAPK module serves only as an attenuator, regardless of phosphatase expression levels. Taken together, the module may operate as a signal amplifier or attenuator.

The results from the model demonstrate that the kinase module may operate as both an amplifier and attenuator (Figure II-6). At high values of π_s , the cascade always attenuates signal, even if downstream kinases outnumber upstream activators. Under these conditions, deactivators considerably outnumber activators, and signal production at each stage is strongly inhibited. In turn, low levels of kinase activation at each stage

reduces the driving force for activation in the next stage, thereby diminishing signal strength across the cascade. Hence, even if downstream kinases outnumber upstream activators, amplification is not assured.

In the other extreme, as $\pi_s \rightarrow 0$, there is no restraint on kinase activation, and all available enzymes in each stage of the cascade are activated. The fraction of enzymes activated at each stage asymptotes to one (i.e., $Erk_{ss}^* \rightarrow 1$), and signal gain across the module approaches a value dictated solely by the relative expression levels of kinases and input magnitude:

$$\lim_{\pi_s \rightarrow 0} \Gamma = \frac{Erk_T}{I^* I_T} = \frac{1}{I^*} \left(\frac{Raf_T}{I_T} \right) \left(\frac{Mek_T}{Raf_T} \right) \left(\frac{Erk_T}{Mek_T} \right) \quad (22)$$

In the case of equimolar expression level ($\kappa_s = 1$), the gain asymptotes to $1/I^*$. Thus, even for equimolar expression level of kinases, amplification is guaranteed provided all input species are not in their active state (i.e., $I^* < 1$).

4.2-4 Transient input and module dynamics

The module input represents upstream molecule(s) such as active Ras, which governs Raf activation. In many experimental systems, this upstream component undergoes transient activation and is better represented by a pulse, rather than a step input. To examine module performance to a transient input, a pulse input with lifetime δ and amplitude I_o as follows was utilized:

$$I^* = \begin{cases} I_o, & 0 \leq \tau < \delta \\ 0, & \tau \geq \delta \end{cases} \quad (23)$$

The pulse input is represented by instantaneous activation and deactivation. Furthermore, δ is chosen as the time required for the system to reach pseudo-steady state upon receiving input I_o . Thus, system response to loss of input may be analyzed independent of system response to receiving input.

Upon instantaneous input decay, the fraction of Erk in its active state also decays back to basal level as shown in Figure II-7 for fixed π_s and κ_s . Signal decay requires constitutive expression of phosphatases, since reducing the relative amount of these deactivators by decreasing π_s extends signal duration (Figure II-7, compare solid lines). Notably, signal decay is also retarded if more upstream kinases are present relative to downstream targets. Thus, a two-fold increase in κ_s significantly extends signal lifetime (compare solid and dotted lines).

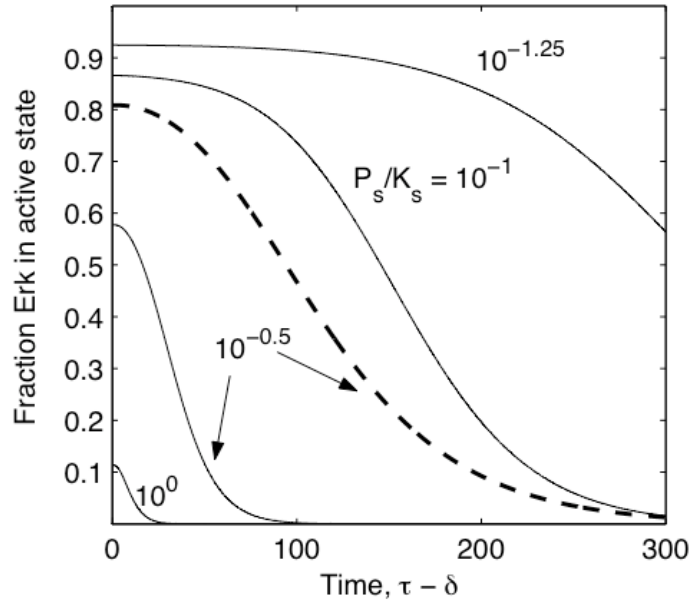


Figure II-7. Temporal profile of module output following instantaneous loss of input.

Upon removal of input at time δ , the module output decays to a basal level in a two-phase process, involving an initial time-lag during which output does not change dramatically, followed by an active decay phase. For fixed $\kappa_s = 1$, reducing the amount of constitutive phosphatases relative to kinases ($\pi_s = 10^{-1.25}$) significantly delays output decay. Thus, instantaneous loss of input enables complete adaptation of module output, provided constitutive phosphatases are expressed. In addition, even for a decay-permissive level of $\pi_s = 10^{-0.5}$, doubling the ratio of upstream to downstream kinase expression extends the lifetime of module output (—).

Although a reduction in π_s or an increase in κ_s elevates output lifetime, these parameter changes also increase the level of output from which decay occurs. To determine whether the rate of signal decay is truly affected or whether extended signal lifetime is a byproduct of starting from a higher output, the temporal decay profiles were recast in a semilog plot (Figure II-8). Beyond a time-lag and during the decay phase, $\log(\text{Erk}^*)$ decreases linearly with time, consistent with a decay rate that is first-order

with respect to fraction of Erk in its active state (Erk^*). Importantly, the slope of this output decay, which is the apparent decay rate constant, is directly affected by changes in π_s and κ_s , showing that extended lifetime is not simply a byproduct of starting from a higher output signal.

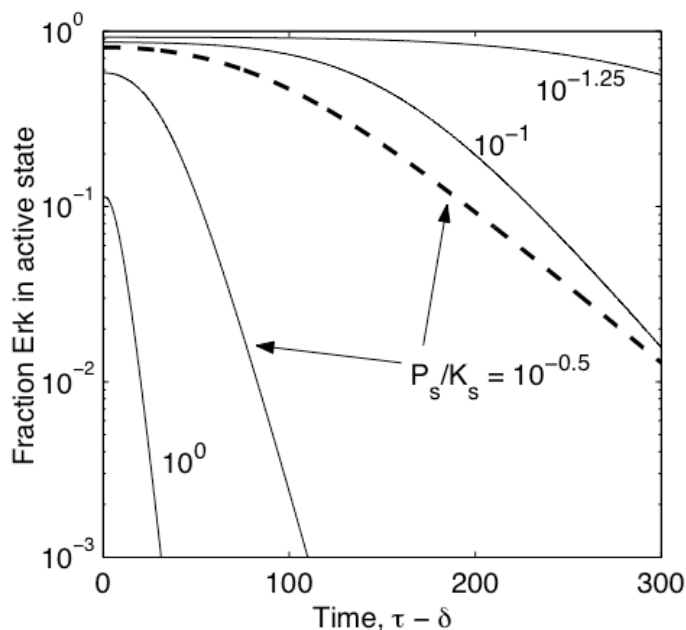


Figure II-8. Output decay in semi-log format.

The decay curves from Figure II-7 are shown on a semilog plot. During the active decay phase, $\log(Erk^*)$ decreases linearly with time, indicating a first-order process with respect to active Erk. Moreover, both π_s and κ_s determine the slope of this linear relationship—the apparent rate constant.

To better understand the relationship between decay rates of input and output, the instantaneous input decay was replaced with an exponential decay characterized by a half-life, $\tau_{1/2}^{input}$. In response, the half-life of module output was calculated for different values of π_s and κ_s . Consistent with above results, increasing π_s or decreasing κ_s

reduces the half-life of module output (Figure II-9). However, this half-life is bounded by a lower limit, which approaches the half-life of the decaying input, emphasizing that this form of adaptation is fully dependent on loss of input.

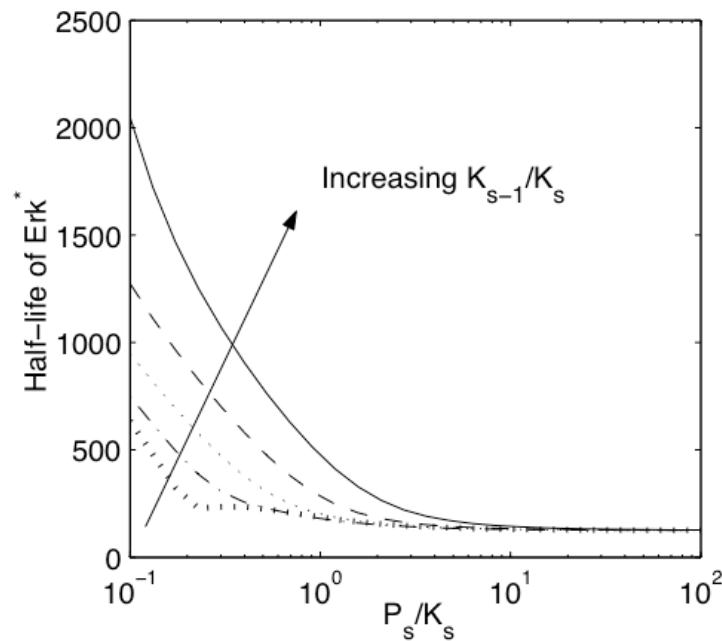


Figure II-9. Half-life of Erk signal in response to an exponential decay in input.

Input amplitude (I^*) was reduced exponentially with an arbitrary, non-zero half-life, $\tau_{1/2}^{input} = 100$. The time for module output to decay to 50% of its initial level was calculated for various π_s and κ_s values. While this half-life of active Erk may be reduced, its lower bound is set by the half-life of input decay. $\kappa_s = 10^{-0.5}$ (||), $10^{-0.25}$ (-.-), 10^0 (...), $10^{0.25}$ (---), $10^{0.5}$ (-).

4.3 Resistance to activation

It is evident that the dimensionless parameters π_s and κ_s have opposing effects on both steady-state properties and signal dynamics (refer to Figure II-4, Figure II-5, Figure II-6, and Figure II-9). These two ratios capture the competing effects that

phosphatases and upstream activators exert on kinase activity at each stage of the cascade. To determine if a single parameter accurately integrates these opposing effects, we defined a combined parameter as follows:

$$\Omega_s = (P_s/K_s)/(K_{s-1}/K_s) = \pi_s/\kappa_s. \quad (24)$$

This parameter represents the expression level of phosphatase (P_s) relative to the total amount of upstream kinase (K_{s-1}), offering a net measure of resistance to signal activation at each stage of the cascade. The present treatment maintains that all stages have the same resistance, allowing overall module resistance to be equated to resistance at each stage.

To determine if this metric of resistance accurately predicts module behavior, the dependence of signal half-life on Ω_s was examined. The half-life of output in response to an exponential decay in input was presented for independent variations in κ_s and π_s in Figure II-9. These data collapse into a single dependence on resistance to activation (Figure II-10), indicating that effects of changing κ_s and π_s may be predicted by the correlating parameter, Ω_s . As resistance to activation increases, module output is more easily diminished, thereby reducing the half-life of signal. In fact, the predictive utility of this metric of resistance is robust. Thus, for values of the rate constant-embedded dimensionless groups (α_i , ε_i , κ_i) that span a range of two orders of magnitude, the resistance quantitatively predicts signal half-life in response to changes in κ_s and π_s (see Appendix).

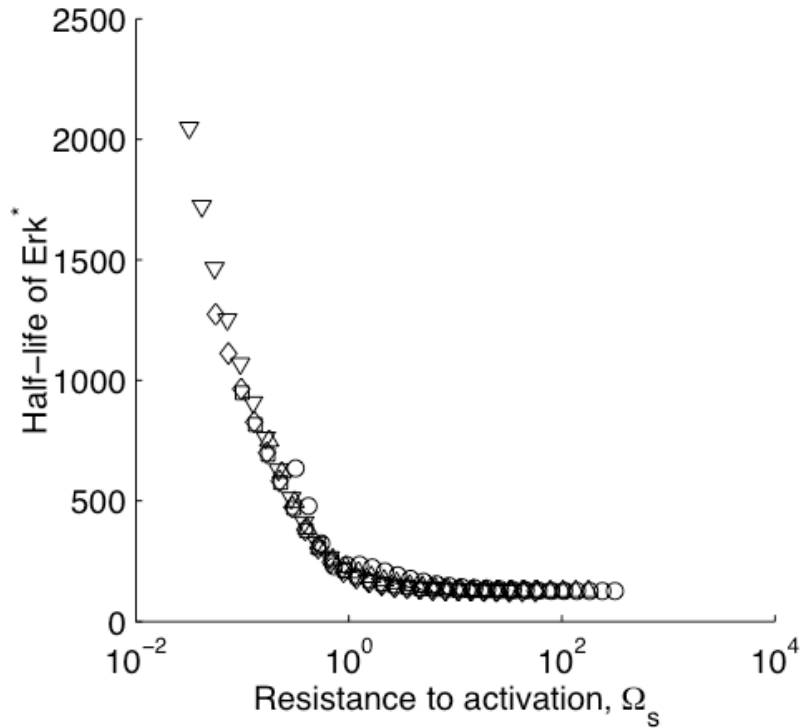


Figure II-10. The dependence of half-life of Erk signal on the resistance to activation for wide range of perturbations in π_s and κ_s .

The half-life of module output depicted in Figure II-9 for $\pi_s = 10^{-1} - 10^2$ and $\kappa_s = 10^{-0.5}$ (O), $10^{-0.25}$ (Δ), 10^0 (□), $10^{0.25}$ (◇), $10^{0.5}$ (∇) have been plotted as a function of module resistance, $\Omega_s = \pi_s / \kappa_s$. A single relationship is revealed between half-life of active Erk and resistance, encompassing all changes in π_s and κ_s .

Additionally, the resistance to activation accurately predicts steady-state features such as module range and input potency. As shown in Figure II-11, at low resistance, even the smallest input produces maximum output, limiting module range. Conversely, high resistance to deactivation impedes signal production even at maximum input. Only at an intermediate resistance, the opposing effects of upstream activators and phosphatases are balanced to yield maximum range of module output. However, at a

resistance ($\Omega_s \approx 10^{-1}$) that is optimal for output range, the input potency is reduced by approximately 1.5 orders of magnitude (Figure II-12).

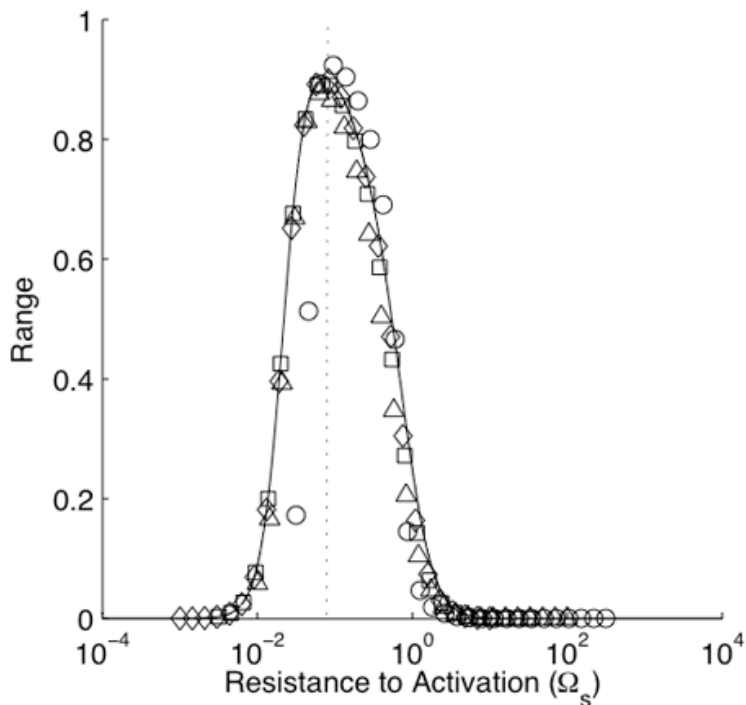


Figure II-11. The dependence of dynamic range of module output on resistance to activation for wide range of perturbations in π_s and κ_s .

Output range, which was depicted in Figure II-5 for $\pi_s = 10^{-2} - 10^2$ and $\kappa_s = 10^{-0.5}$ (O), 10^0 (Δ), $10^{0.5}$ (\square), 10^1 (\diamond), shows a single, biphasic relationship to resistance to activation. Thus, maximum range may be obtained by adjusting either π_s or κ_s to net a resistance $\Omega_s \approx 10^{-1}$ (dotted line). The solid black line shows the analytic solution of the range for a three stage cascade.

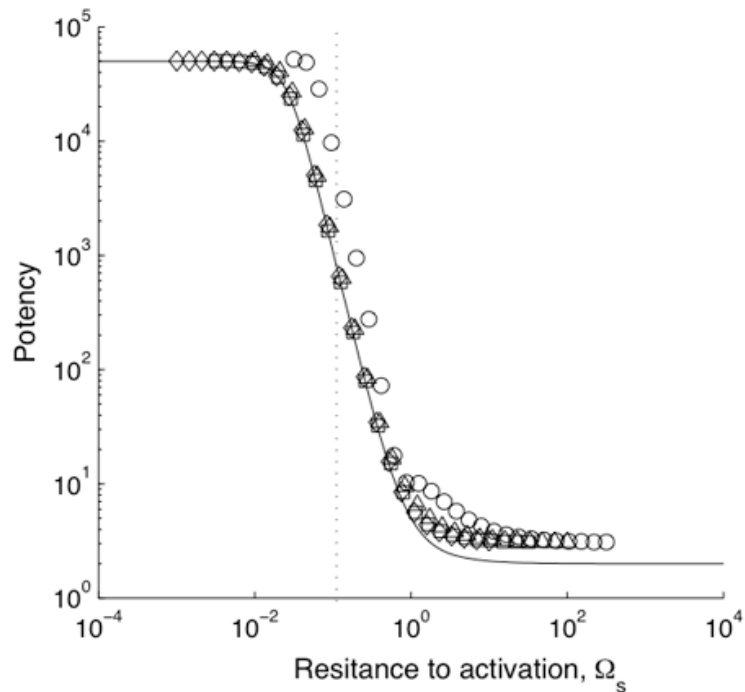


Figure II-12. The dependence of input potency on resistance to activation for wide range of perturbations in π_s and κ_s .

Input potency, which was depicted in Figure II-4 for $\pi_s = 10^{-2} - 10^2$ and $\kappa_s = 10^{-0.5}$ (O), 10^0 (Δ), $10^{0.5}$ (\square), 10^1 (\diamond), shows a single, monotonically decreasing relationship to resistance to activation. At an intermediate resistance that optimizes module range (dotted line), input potency is at least one order of magnitude below its maximum. The solid black line shows the analytic solution of the potency for a three stage cascade.

4.4 Relaxation of resistance parameters

The previous results were subject to the constraint that a single resistance (Ω_s) was uniformly applied to all stages of the MAP kinase module. We relaxed this constraint to allow unequal stage resistances ($\omega_1, \omega_2, \omega_3$). To describe the behavior of the MAP kinase cascade with variable stage resistances, we first focused analytically on the performance of a single stage in isolation. (For consistent nomenclature, we used Raf activation in isolation from the rest of the cascade to illustrate our derivation of single

stage resistance.) Previous work by Goldbeter and Koshland appropriately described the steady-state behavior of such a single stage system (Goldbeter and Koshland, 1981). To arrive at their solution, the authors made two key assumptions. First, they neglected the contribution of $\{I^* \cdot Raf\}$ and $\{P_{Rf} \cdot Raf^*\}$ to the species balance of the substrate, Raf. Second, they assumed that the converter enzymes, I^* and P_{Rf} , operate in the first order regime, or that

$$Raf_T \ll \frac{k_{-1} + k_{cat,1}}{k_{+1}} \text{ and } Raf_T \ll \frac{k_{-4} + k_{cat,4}}{k_{+4}} \quad (25)$$

The following analytical expression describes the steady-state activation of the modified substrate (Raf_{ss}^*) as a function of the rate constants and the total concentrations of the model components, where we have recast the equation using our dimensionless groups:

π_s , κ_s , α_i , ε_i and τ_i .

$$Raf_{ss}^* = \frac{1}{1 + \omega_1 \frac{K_{M,1}}{K_{M,4}} \left(\frac{1}{I^*} \right)}, \text{ where } K_{M,i} = \frac{\tau_i(1 + \varepsilon_i)}{\alpha_i/\kappa_s} \text{ and } \omega_s = \frac{\pi_s}{\kappa_s} \quad (26)$$

Note that the single stage resistance, ω_1 , falls cleanly out of the above equation, as suggested from our prior computational results. Generalizing this result to the second and third stages of the cascade, we obtain the following equations:

$$Mek_{ss}^* = \frac{1}{1 + \omega_2 \frac{K_{M,2}}{K_{M,5}} \left(\frac{1}{Raf^*} \right)} \quad (27)$$

$$Erk_{ss}^* = \frac{1}{1 + \omega_3 \frac{K_{M,3}}{K_{M,6}} \left(\frac{1}{Mek^*} \right)} \quad (28)$$

Now, to reconstruct an n-stage cascade using the above equations, it must further be assumed that there are no upstream interactions, i.e., the parameters and potential behavior of stage $s + 1$ does not influence the behavior of stage s . Then, the above equation can be iteratively substituted into itself to obtain a steady-state dose-response expression for any n-stage cascade. Following are the first three iterations:

$$Raf_{ss}^* = \frac{1}{1 + \omega_1 \frac{K_{M,1}}{K_{M,4}} \left(\frac{1}{I^*} \right)} \quad (29)$$

$$Mek_{ss}^* = \frac{1}{1 + \omega_2 \frac{K_{M,2}}{K_{M,5}} \left(1 + \omega_1 \frac{K_{M,1}}{K_{M,4}} \left(\frac{1}{I^*} \right) \right)} \quad (30)$$

$$Erk_{ss}^* = \frac{1}{1 + \omega_3 \frac{K_{M,3}}{K_{M,6}} \left(1 + \omega_2 \frac{K_{M,2}}{K_{M,5}} \left(1 + \omega_1 \frac{K_{M,1}}{K_{M,4}} \left(\frac{1}{I^*} \right) \right) \right)} \quad (31)$$

The above dose-response curves can now be used to quantitatively predict any steady-state property of the cascade, including the dynamic range and potency. The dynamic range can be obtained in a straightforward manner by substituting Equation 30 or 31 into Equation 20. Below are the analytic equations for the range of a 2-stage and a 3-stage cascade:

$$\text{range}_{s=2} = \frac{1}{1 + \omega_2 \frac{K_{M,2}}{K_{M,5}} \left(1 + \omega_1 \frac{K_{M,1}}{K_{M,4}} \left(\frac{1}{I_{\max}^*} \right) \right)} - \frac{1}{1 + \omega_2 \frac{K_{M,2}}{K_{M,5}} \left(1 + \omega_1 \frac{K_{M,1}}{K_{M,4}} \left(\frac{1}{I_{\min}^*} \right) \right)} \quad (32)$$

$$\begin{aligned} \text{range}_{s=3} = & \frac{1}{1 + \omega_3 \frac{K_{M,3}}{K_{M,6}} \left(1 + \omega_2 \frac{K_{M,2}}{K_{M,5}} \left(1 + \omega_1 \frac{K_{M,1}}{K_{M,4}} \left(\frac{1}{I_{\max}^*} \right) \right) \right)} - \dots \\ & \dots - \frac{1}{1 + \omega_3 \frac{K_{M,3}}{K_{M,6}} \left(1 + \omega_2 \frac{K_{M,2}}{K_{M,5}} \left(1 + \omega_1 \frac{K_{M,1}}{K_{M,4}} \left(\frac{1}{I_{\min}^*} \right) \right) \right)} \end{aligned} \quad (33)$$

Equation 33 precisely recapitulates the results from our numerical simulations for the same values of π_s and κ_s (Figure II-11). Using Equation 32 for a 2-stage cascade, we computed the dynamic range where ω_1 and ω_2 vary independently of each other (Figure II-13). We chose to show this result for a 2-stage cascade so that the results could be displayed graphically. The model predicted that the dynamic range will depend on both ω_1 and ω_2 and that there is a region in the ω_1, ω_2 plane for which the range is biologically significant (i.e., where the range is near 1).

Likewise, the potency can be described by an analytic expression derived from Equations 30 and 31. Given a certain dynamic range determined by I_{min} and I_{max} , the potency is equal to the I/I^* that gives half-maximal response within the dynamic range; the potency is therefore a function of I_{min} , I_{max} , ω_s , and $K_{M,i}$. The potency has been derived for a 2-stage and a 3-stage cascade as follows:

$$potency_{s=2} = \frac{1}{2} \left(\frac{1}{I_{max}} + \frac{1}{I_{min}} \right) \frac{\left(1 + \omega_2 \frac{K_{M,2}}{K_{M,5}} \left(1 + \omega_1 \frac{K_{M,1}}{K_{M,4}} \left(\frac{2}{I_{max} + I_{min}} \right) \right) \right)}{\left(1 + \omega_2 \frac{K_{M,2}}{K_{M,5}} \left(1 + \omega_1 \frac{K_{M,1}}{K_{M,4}} \frac{1}{2} \left(\frac{1}{I_{max}} + \frac{1}{I_{min}} \right) \right) \right)} \quad (34)$$

$$potency_{s=3} = \frac{1}{2} \left(\frac{1}{I_{max}} + \frac{1}{I_{min}} \right) \frac{\left(1 + \omega_3 \frac{K_{M,3}}{K_{M,6}} \left(1 + \omega_2 \frac{K_{M,2}}{K_{M,5}} \left(1 + \omega_1 \frac{K_{M,1}}{K_{M,4}} \left(\frac{2}{I_{max} + I_{min}} \right) \right) \right) \right)}{\left(1 + \omega_3 \frac{K_{M,3}}{K_{M,6}} \left(1 + \omega_2 \frac{K_{M,2}}{K_{M,5}} \left(1 + \omega_1 \frac{K_{M,1}}{K_{M,4}} \frac{1}{2} \left(\frac{1}{I_{max}} + \frac{1}{I_{min}} \right) \right) \right) \right)} \quad (35)$$

Equation 35 is plotted in Figure II-12, and accurately recapitulates the results from our numerical simulations. To characterize the variation of the potency with single stage resistance, we plotted Equation 34 as a function of both ω_1 and ω_2 (Figure II-14). As

anticipated, the potency is maximized when both ω_1 and ω_2 are small. Comparing both the range and the potency for a 2-stage cascade, we observe that both properties cannot be simultaneously optimized by altering the resistance vector, (ω_1, ω_2) . Rather, a balance must be achieved that permits an appropriately large dynamic range to communicate with downstream modules, while having an adequate potency to sense the input.

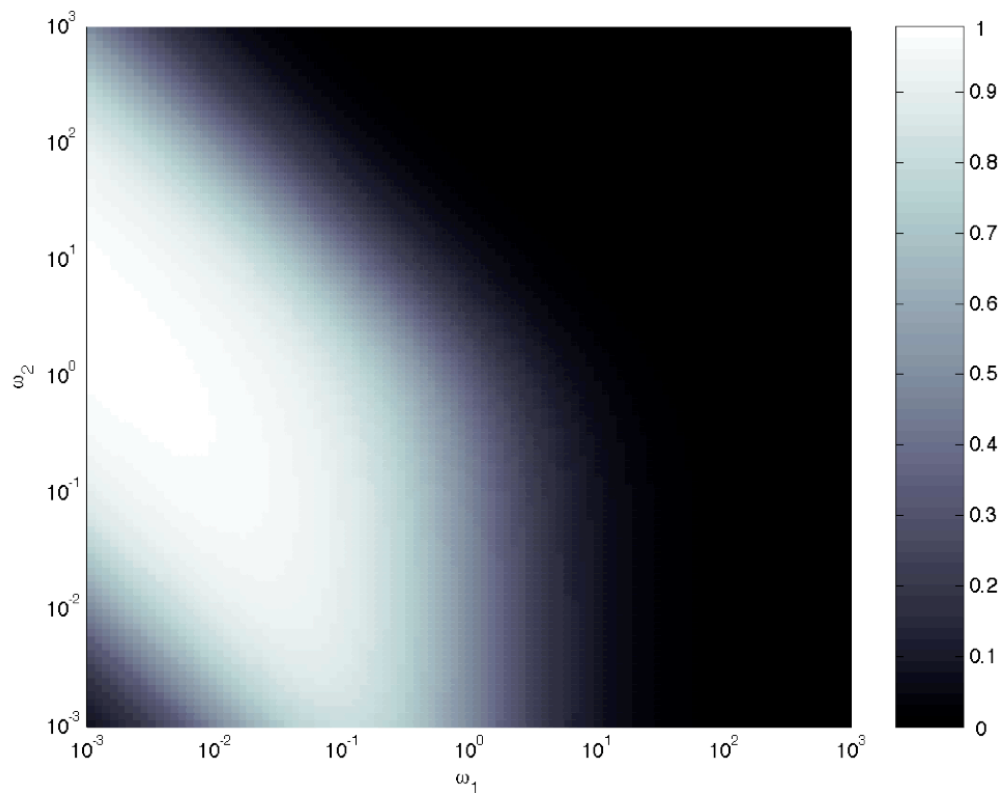


Figure II-13. Dynamic range as a function of single stage resistances.

The analytic solution to the dynamic range for a 2-stage cascade (Equation 32) is plotted as a function of independent resistances, ω_1 and ω_2 . The color intensity indicates the value of the range.

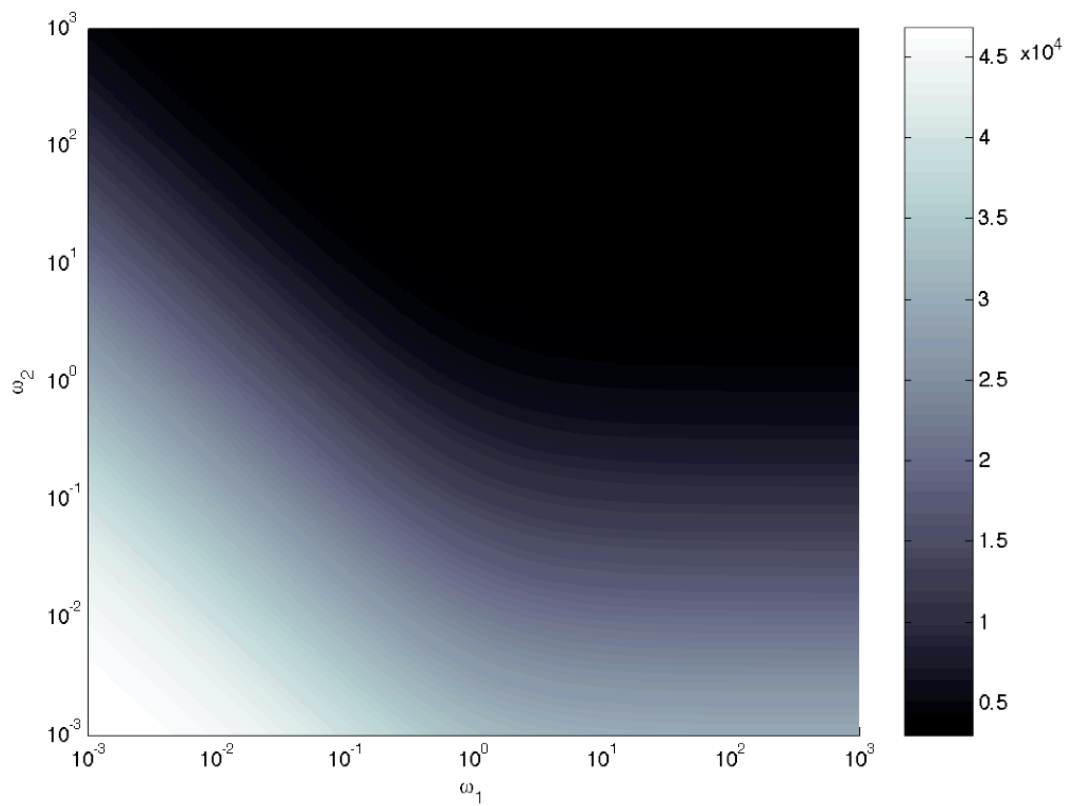


Figure II-14. Potency as a function of single stage resistances.

The analytic solution to the input postency for a 2-stage cascade (Equation 34) is plotted as a function of independent resistances, ω_1 and ω_2 . The color intensity indicates the value of the potency.

5. *Discussion*

The MAP kinase module is a recurring mode of signal transduction utilized in natural systems to regulate cell proliferation, differentiation, migration and gene expression (Lewis et al., 1998; Pearson et al., 2001). Therefore, re-engineering this module's quantitative signaling properties would offer powerful means to control a range of cell behaviors. Two important issues emerge when developing strategies to re-engineer signaling networks. First, the quantitative features most attractive to redesign must be identified. Second, an understanding as to how these features depend on parts of the circuit that are most amenable to manipulation in experimental systems must be developed. The computational analysis presented here delineates how features of the MAP kinase module such as signal amplification, range of output and signal lifetime depend on experimentally adjustable components—kinase and phosphatase expression level. Moreover, it is illustrated that the effect of perturbing the expression level of these constituents on the MAP kinase circuit may be accurately predicted through a parameter that gauges resistance to signal activation.

Signal amplification has been viewed classically as a chief function of kinase cascades, especially under conditions where downstream target outnumber upstream kinase as in the case of Raf-Mek signal exchange (Pearson et al., 2001). Model analysis suggests that this sufficiency criteria for amplification represents only a limiting condition in which the amount of kinases greatly exceed phosphatases. In this scenario, even the smallest, non-zero input triggers complete activation of all kinases in the cascade. Thus, output is assured to be greater than input, since the downstream

component is expressed at higher level. However, phosphatases such as HePTP, PP1 and PP2A, which deactivate module kinases, are expressed constitutively in many cell systems (Keyse, 2000; Saxena and Mustelin, 2000; Tamura et al., 2002). In their presence, the model predicts that even modules with greater downstream components than upstream activators may perform as attenuators. This is consistent with measurements in both yeast and mammalian cells in which signal gain is often orders-of-magnitude lower than that predicted by knowledge of relative kinase expression level alone (Ferrell, 1996). Therefore, the important parameter is not only the relative amount of upstream to downstream factors (κ_s), but also the amount of phosphatase relative to kinase (π_s) at each stage s of the cascade.

Integrating the contributions from these two parameters, the resistance to signal activation at each stage (Ω_s) effectively gauges module capacity to transduce signal. Large values for Ω_s represent greater resistance to signal activation, impeding module response to input. One gauge of input effectiveness is its potency, which measures the amount of input required to induce half-maximal response. A single, monotonically decreasing function describes the dependence of input potency on resistance to signal activation, despite independently varying the ratio of upstream to downstream kinase amount or relative level of phosphatases and kinases. At low resistance, efficient output is produced even for small input values, thereby conferring high potency to the input.

This result would suggest that a module design with kinases and relatively minimal phosphatases would offer the strongest response to input. However, while input

potency may be enhanced by reducing resistance to activation, there is a design trade-off involving another feature—the range of output with which the module communicates to potential downstream effectors. A discrete number of active Erk molecules serve as module output. If output is a graded function of input amount, the range represents intermediate amounts of active MAP kinase with which the module may relay higher-grain information to downstream targets. Alternatively, the MAP kinase cascade may function as a switch, toggling between an on- and off-state (Huang and Ferrell, 1996). In this case, maximum range is desirable, since it dictates the ease with which downstream effectors resolve between on- and off-states. Unlike input potency, module range is a biphasic function of resistance to activation. At low and high resistances, module output is either too easily stimulated to maximum or too difficult to activate beyond near-zero response, respectively. To maximize range, an intermediate resistance to activation is required, but at the cost of input potency. Importantly, the resistance to signal activation offers predictive value in assessing this design trade-off between enhancing communication with input (input potency) versus downstream effectors (range).

In addition to steady-state features, module resistance to activation serves as a predictive tool for redesigning signal dynamics. Since transient MAP kinase signals elicit different cell behaviors than sustained signals (Marshall, 1995; Roulston et al., 1998), tuning signal lifetime has direct implications for engineering cell behavior. Model analysis indicates two regimes of control over signal lifetime. In the first regime, resistance to activation is high, ensuring rapid signal decay. In this case, input and output decay with similar kinetics, and further increasing resistance will not reduce signal

lifetime. This prediction of input-dictated control of signal lifetime is consistent with regulatory schemes employed in natural systems. In PC12 cells, EGF transiently activates Erk and promotes proliferation, while NGF-mediated sustained Erk activation leads to differentiation (Marshall, 1995). Underlying this difference, EGF drives Erk activation via an unstable protein complex including Crk, C3G and Rap1, while NGF-mediated input to the Erk module involves a stable form of the same complex (Kao et al., 2001). Hence, regulating input stability has been proposed to mediate differences in module output dynamics. Model predictions would further suggest an important role for constitutive phosphatase activity in such systems, since module resistance to signal activation is required for transient input to produce transient output.

The second regime of control over dynamics occurs at low or intermediate resistances at which input decays more rapidly than output. In this case, the time-scale of MAP kinase signal decay will be sensitive to an increase in module resistance to activation. Similar to other signaling systems in which signal adapts despite continued presence of input (Alon et al., 1999; Barkai and Leibler, 1997; Yi et al., 2000), decay of this module's output in response to a transient input is a robust property, but the time to achieve complete decay is not. In fact, this flexibility is likely exploited by natural systems, in which external stimuli not only activate kinases, but also alter phosphatase expression and/or their enzymatic activity (Keyse, 2000; Saxena and Mustelin, 2000; Tamura et al., 2002). Model results indicate that such changes would modify the resistance to signal propagation, altering signal lifetime based on environmental context. Since choice of cell behavior has been linked to MAP kinase signal dynamics, this offers

an adaptable platform to produce quantitatively distinct signals with disparate functional outcomes using a single signaling module. Such flexibility is consistent with the pleiotropic effects that individual MAP kinases exert on cell function. Furthermore, similar phosphatase-mediated flexibility has been reported in a larger scale network, which includes pathways extrinsic to the MAP kinase module involving Erk-mediated negative and positive feedback (Asthagiri and Lauffenburger, 2001; Bhalla et al., 2002).

In summary, this work delineates features of the MAP kinase module that are attractive targets for engineering design. Moreover, it is proposed that these features may be tuned in a predictable fashion by considering a single metric—the resistance to activation. Future work will focus not only on implementing these design strategies in experimental systems, but also to exploit the modular character of our model, which focuses on mechanisms intrinsic to the MAP kinase cascade. Such modular models are an important first-step in a hierarchical strategy to represent large signal networks through interconnected modules in a manner analogous to the construction of a circuit board of interconnected integrated chips (Asthagiri and Lauffenburger, 2000). To be effective, hierarchical models require that the mechanistic, detailed description of individual modules be substituted with computationally less intensive, yet quantitative, “operating rules.” This computational work offers such a description for the MAP kinase module by reducing the combined contributions of kinases and phosphatases into a single metric, which gauges resistance to signal activation and accurately predicts several quantitative module features. Interconnecting such analog rules for information processing, along with Boolean operations characteristic of other biochemical networks (Arkin and Ross,

1994), may help to form a quantitative basis for model reduction of large signaling networks.

6. Appendix

The resistance to activation accurately predicts signal half-life over a wide range of values for π_s and κ_s (see Figure II-10). Here, we examined the robustness of this predictive capability to changes in the dimensionless groups that involve rate constants, namely α_i , ε_i , τ_i . Sensitivity to each parameter was performed by varying its value over two orders of magnitude around its reference value (see Table II-1).

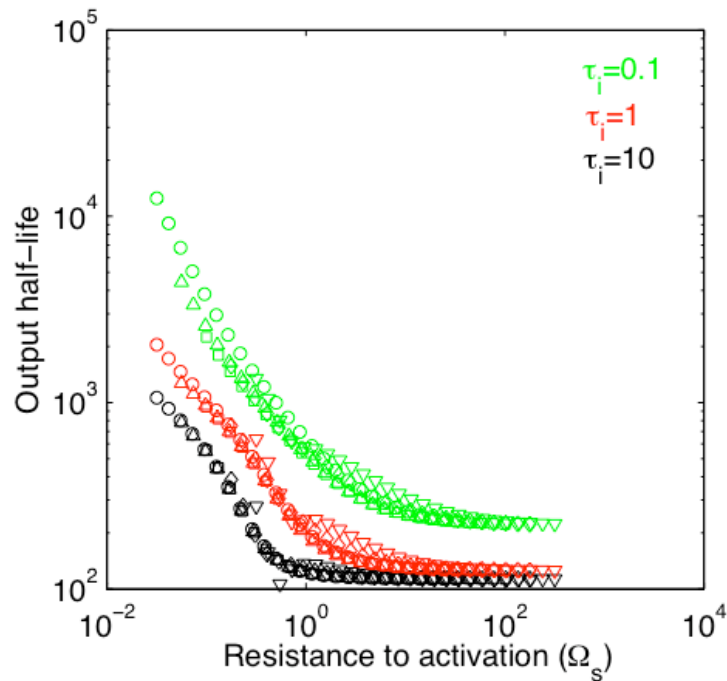


Figure II-15. Sensitivity analysis of the ability of module resistance to predict half-life due to changes in π_s and κ_s for perturbations in τ_i .

The value of τ_i was varied among 0.1 (green), 1 (red) and 10 (black). The parameters π_s and κ_s were varied over the same range as in Figure II-10, i.e., $\pi_s = 10^{-1} - 10^2$ and $\kappa_s = 10^{-0.5}$ (∇), $10^{-0.25}$ (\diamond), 10^0 (\square), $10^{0.25}$ (Δ), $10^{0.5}$ (O).

As expected, for fixed π_s and κ_s , decreasing τ_i changes the half-life of output signal (Figure II-15). Notably, for each value of τ_i (0.1, 1 and 10 with each grouped by color), module resistance accurately predicts half-life for wide perturbations in the potential design variables— π_s and κ_s . Similar robustness in the ability of module resistance to predict signal half-life for changes in π_s and κ_s is observed for perturbations in ε_i and α_i (Figure II-16 and Figure II-17, respectively).

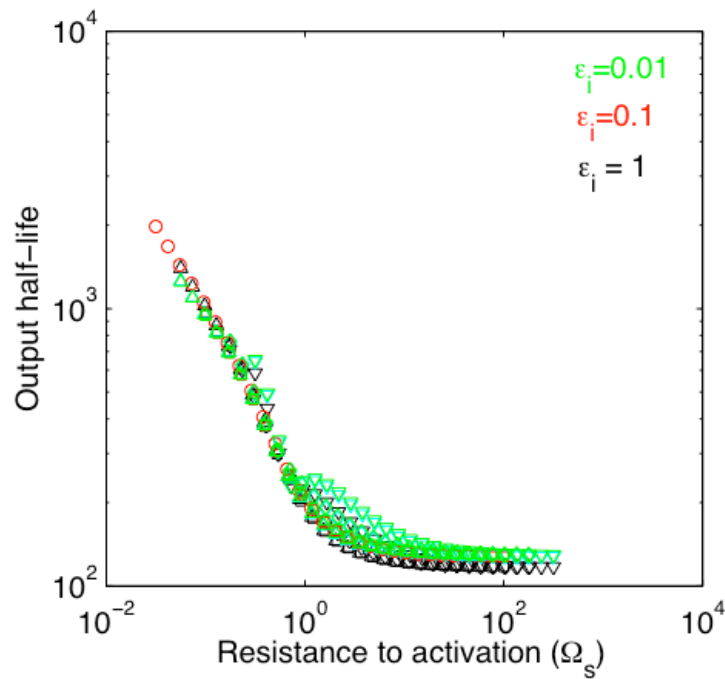


Figure II-16. Sensitivity analysis of the ability of module resistance to predict half-life due to changes in π_s and κ_s for perturbations in ε_i .

The value of ε_i was varied among 0.01 (green), 0.1 (red) and 1 (black). The parameters π_s and κ_s were varied over the same range as in Figure II-10, i.e., $\pi_s = 10^{-1} - 10^2$ and $\kappa_s = 10^{-0.5} (\nabla)$, $10^{-0.25} (\diamond)$, $10^0 (\square)$, $10^{0.25} (\Delta)$, $10^{0.5} (O)$.

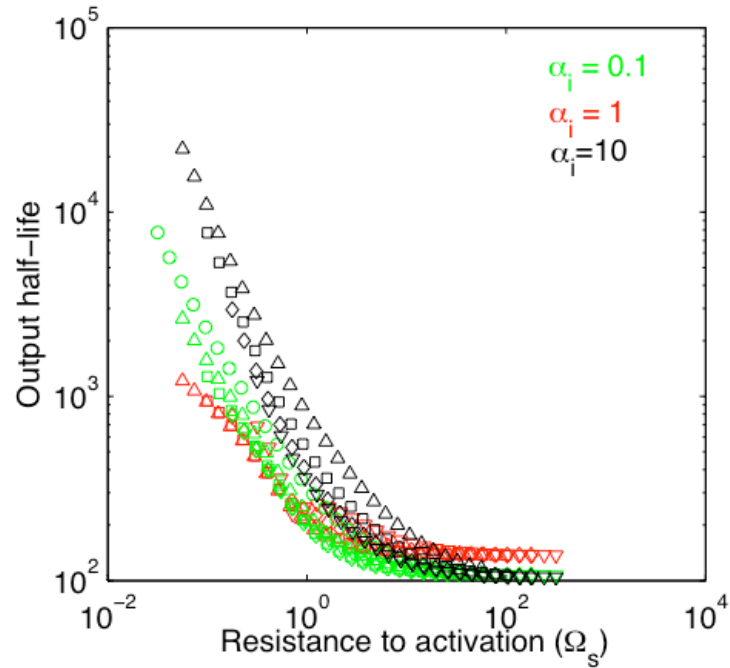


Figure II-17. Sensitivity analysis of the ability of module resistance to predict half-life due to changes in π_s and κ_s for perturbations in α_i .

The value of α_i was varied among 0.1 (green), 1 (red) and 10 (black). The parameters π_s and κ_s were varied over the same range as in Figure II-10, i.e., $\pi_s = 10^{-1} - 10^2$ and $\kappa_s = 10^{-0.5}$ (∇), $10^{-0.25}$ (\diamond), 10^0 (\square), $10^{0.25}$ (Δ), $10^{0.5}$ (\circ).

7. Acknowledgements

The authors thank M. Davis and P. Sternberg for critical review of the manuscript. Financial support was provided by the California Institute of Technology and the Institute for Collaborative Biotechnologies through grant DAAD 19-13-D-0004 from the U.S. Army Research Office.

8. References

- Alon, U., M.G. Surette, N. Barkai, and S. Leibler. 1999. Robustness in bacterial chemotaxis. *Nature*. 397:168-71.
- Arkin, A., and J. Ross. 1994. Computational functions in biochemical reaction networks. *Biophys J*. 67:560-78.
- Asthagiri, A.R., and D.A. Lauffenburger. 2000. Bioengineering models of cell signaling. *Annu Rev Biomed Eng*. 2:31-53.
- Asthagiri, A.R., and D.A. Lauffenburger. 2001. A computational study of feedback effects on signal dynamics in a mitogen-activated protein kinase (MAPK) pathway model. *Biotechnol Prog*. 17:227-39.
- Barkai, N., and S. Leibler. 1997. Robustness in simple biochemical networks. *Nature*. 387:913-7.
- Bhalla, U.S., P.T. Ram, and R. Iyengar. 2002. MAP kinase phosphatase as a locus of flexibility in a mitogen-activated protein kinase signaling network. *Science*. 297:1018-23.
- Brown, G.C., J.B. Hoek, and B.N. Kholodenko. 1997. Why do protein kinase cascades have more than one level? *Trends Biochem Sci*. 22:288.
- Davis, R.J. 2000. Signal transduction by the JNK group of MAP kinases. *Cell*. 103:239-52.
- Endy, D., and R. Brent. 2001. Modelling cellular behaviour. *Nature*. 409:391-5.
- Ferrell, J.E., Jr. 1996. Tripping the switch fantastic: how a protein kinase cascade can convert graded inputs into switch-like outputs. *Trends Biochem Sci*. 21:460-6.

- Ferrell, J.E., Jr. 1997. How responses get more switch-like as you move down a protein kinase cascade. *Trends Biochem Sci.* 22:288-9.
- Goldbeter, A., and D.E. Koshland, Jr. 1981. An amplified sensitivity arising from covalent modification in biological systems. *Proc Natl Acad Sci U S A.* 78:6840-4.
- Huang, C.Y., and J.E. Ferrell, Jr. 1996. Ultrasensitivity in the mitogen-activated protein kinase cascade. *Proc Natl Acad Sci U S A.* 93:10078-83.
- Kao, S., R.K. Jaiswal, W. Kolch, and G.E. Landreth. 2001. Identification of the mechanisms regulating the differential activation of the mapk cascade by epidermal growth factor and nerve growth factor in PC12 cells. *J Biol Chem.* 276:18169-77.
- Keyse, S.M. 2000. Protein phosphatases and the regulation of mitogen-activated protein kinase signalling. *Curr Opin Cell Biol.* 12:186-92.
- Levchenko, A., J. Bruck, and P.W. Sternberg. 2000. Scaffold proteins may biphasically affect the levels of mitogen-activated protein kinase signaling and reduce its threshold properties. *Proc Natl Acad Sci U S A.* 97:5818-23.
- Lewis, T.S., P.S. Shapiro, and N.G. Ahn. 1998. Signal transduction through MAP kinase cascades. *Adv Cancer Res.* 74:49-139.
- Marshall, C.J. 1995. Specificity of receptor tyrosine kinase signaling: transient versus sustained extracellular signal-regulated kinase activation. *Cell.* 80:179-85.
- Pages, G., P. Lenormand, G. L'Allemain, J.C. Chambard, S. Meloche, and J. Pouyssegur. 1993. Mitogen-activated protein kinases p42mapk and p44mapk are required for fibroblast proliferation. *Proc Natl Acad Sci U S A.* 90:8319-23.

- Park, S.H., A. Zarrinpar, and W.A. Lim. 2003. Rewiring MAP kinase pathways using alternative scaffold assembly mechanisms. *Science*. 299:1061-4.
- Pearson, G., F. Robinson, T. Gibson, B.-E. Xu, M. Karandikar, K. Berman, and M. Cobb. 2001. Mitogen-activated protein (MAP) kinase pathways: Regulation and physiological functions. *Endocrine Reviews*. 22:153-183.
- Roulston, A., C. Reinhard, P. Amiri, and L.T. Williams. 1998. Early activation of c-Jun N-terminal kinase and p38 kinase regulate cell survival in response to tumor necrosis factor alpha. *J Biol Chem*. 273:10232-9.
- Saxena, M., and T. Mustelin. 2000. Extracellular signals and sources of phosphatases: all roads lead to MAP kinase. *Semin Immunol*. 12:387-96.
- Scheele, J.S., J.M. Rhee, and G.R. Boss. 1995. Determination of absolute amounts of GDP and GTP bound to Ras in mammalian cells: comparison of parental and Ras-overproducing NIH 3T3 fibroblasts. *Proc Natl Acad Sci U S A*. 92:1097-100.
- Schoeberl, B., C. Eichler-Jonsson, E.D. Gilles, and G. Muller. 2002. Computational modeling of the dynamics of the MAP kinase cascade activated by surface and internalized EGF receptors. *Nat Biotechnol*. 20:370-5.
- Tamura, S., M. Hanada, M. Ohnishi, K. Katsura, M. Sasaki, and T. Kobayashi. 2002. Regulation of stress-activated protein kinase signaling pathways by protein phosphatases. *Eur J Biochem*. 269:1060-6.
- Tyson, J.J., K. Chen, and B. Novak. 2001. Network dynamics and cell physiology. *Nat Rev Mol Cell Biol*. 2:908-16.

Yi, T.M., Y. Huang, M.I. Simon, and J. Doyle. 2000. Robust perfect adaptation in bacterial chemotaxis through integral feedback control. *Proc Natl Acad Sci U S A.* 97:4649-53.